– Cover Page –

Manuscript entitled:

Numerical Estimations of Lightning-Induced Mechanical Damage in Carbon/Epoxy Composites Using Shock Wave Overpressure and Equivalent Air Blast Overpressure

Submitted to:

Composite Structures

Authored by:

Juhyeong Lee, [1, 2*] Thomas E. Lacy, Jr., [3] Charles U. Pittman, Jr., [4] J. N. Reddy [3]

1. Advanced Composites Collaboration for Innovation, University of Bristol, Bristol, BS8 1TR, UK
2. Department of Mechanical and Aerospace Engineering, Utah State University, Logan, UT 84322-4130, USA
3. J. Mike Walker '66 Department of Mechanical Engineering, Texas A&M University, College Station, TX 77843-3127, USA
4. Department of Chemistry, Mississippi State University, Mississippi State, MS 39759, USA

Keywords: Lightning mechanical damage; Shockwave overpressure; Air blast overpressure; Lightning damage prediction.

* Corresponding author

Juhyeong Lee PhD

Research Associate (~04/2019)
Advanced Composites Collaboration for Innovation and Science (ACCIS)
Department of Aerospace Engineering,
University of Bristol, BS8 1TR, Bristol, UK
Email: juhyeong.lee@bristol.ac.uk

Assistant Professor (08/2019~)
Department of Mechanical and Aerospace Engineering
Utah State University
Logan, UT 84322-4130, USA
Email: juhyeong.lee@usu.edu

Abstract

A new approach is proposed for predicting lightning-induced mechanical damage using the shock wave overpressure (SWO) due to lightning arc channel expansion and also its equivalent air blast overpressure (ABO) due to an explosion of chemical potential energy in AS4/3506 carbon/epoxy laminates. The SWOs and equivalent ABOs associated with 124, 247, and 494 kA peak lightning currents were considered. Dynamic responses of the composite laminates due to both the SWOs and ABOs were similar to each other. The spatial variations in the peak compressive and tensile midplane displacements evaluated near the laminate center showed that mechanical damage tended to be symmetric about the laminate midplane. Hashin's four different damage criteria were implemented to predict fiber/matrix failures. The predicted failure index distributions in the carbon/epoxy plies were nearly identical for both SWOs and ABOs. Except for matrix tension failure predicted at the 494 kA peak current, all damage failure indices increased as the peak current increased, but were smaller than unity, implying no mechanical damage initiation due to lightning strike. These FE results suggest that lightning SWO may not cause significant *mechanical* damage and it may be possible to interchangeably use either SWO or ABO to predict lightning-induced mechanical damage.

Introduction

Carbon fiber-reinforced polymer (CFRP) composites are widely used in high-performance aerospace structural applications due to the (1) excellent strength-to-weight ratios enabling higher fuel efficiency, (2) design flexibility leading to easier fabrication of complex geometry parts, and (3) high corrosion resistance that can withstand harsher environments than traditional aerospace-grade metal alloys [1]. According to the US Government Accountability Office aviation safety

report [2], CFRP composites will be used for the next-generation commercial and general aviation (GA) primary structural applications. Already, the fuselage and wing structures of the Airbus A380 [3, 4] and the Boeing 787 [5] are primarily made of CFRP composites.

Lightning is a naturally occurring, high voltage, high current, *transient electrical discharge* between two charged regions with opposite polarities. The frequency of lightning strikes to aircraft strongly depends on geographic locations, environmental conditions (*i.e.*, rain, hail, snow, and thunderstorm), and cruising conditions (*i.e.*, altitude, temperature) [6–12]. A typical commercial aircraft is struck once every 3,000 flight hours, equivalent to about once a year [11]. Similarly, GA aircraft experience lightning strikes every 1,000-3,000 flight hours [12]. Special-purpose military aircraft may be more susceptible to lightning strikes than commercial/GA aircraft since they often operate under more severe environmental conditions.

Lightning creates a highly conductive ionized arc channel for the electric current flow. The massive electrical energy released results in significant structural damage to CFRP composites; these include intense fiber damage, matrix decomposition, widespread minor surface burning/scorching, and/or delamination [6–8]. In addition, lightning-induced electromagnetic interference with onboard electronics may cause malfunction of essential control systems and other relevant components. Most of the electrical energy being transferred at a lightning attachment point is instantaneously dissipated as Joule heating. Peak local arc channel temperatures reach ~ 30,000K [13], and the predicted maximum temperature at the initial lightning attachment location is ≥ 3,000K [14–22]. Simultaneously, some fraction of the electrical energy is converted into mechanical and/or electromagnetic energy. Dynamic mechanical pressure loads due to (1) rapid arc channel radial expansion/shrinkage, (2) transient primary galvanic current flow along outer ply conductive fibers causing electro-magnetic (Lorenz) forces, and (3) magnetically-

induced currents resulting from time-varying magnetic fields can produce considerable mechanical damage that can lead to catastrophic failure.

Several researchers have performed *artificial* lightning strike tests to characterize damage development as a function of current waveform parameters [23–30]. Carbon/epoxy laminates can be constructed using either unidirectional or woven fabric plies. Such laminates each exhibit unique damage features due to different in-plane current flows. For example, the in-plane regions of intense local fiber damage are elliptical in character for unidirectional laminates and semi-circular for woven fabric laminates. Numerous multiphysics-based finite element (FE) models [14–22] have also been developed for predicting lightning damage development in carbon/epoxy composites. These models only predict *thermal* damage development by calculating a rapid temperature rise due to electrical conduction and corresponding Joule heating.

Very few models are available in the literature [13, 31–33] that involve dynamic mechanical pressures as a consequence of electro-magnetic forces and lightning acoustic shock waves. These models did not explicitly explain how mechanical pressure loads are generated from given lightning current waveforms. Due to the complex physics and the probabilistic nature of atmospheric lightning, quantifying the influence of the dynamic mechanical pressures induced by lightning strikes is not straightforward. In addition, such mechanical pressures are dependent not only upon the peak current amplitude, but also by the rise/decay time durations, charge transfer, and the action integral of the given current waveforms [34]. Therefore, a direct conversion from peak current values to dynamic mechanical pressure loads without relevant current waveform parameters remains a key challenge.

This study investigates effects of the shock wave overpressures (SWOs) and equivalent air blast overpressures (ABOs), associated with 124, 247, and 494 kA peak lightning currents, on

mechanical damage in 16-ply quasi-isotropic, $[45/0/-45/90]_{2S}$, AS4/3506 carbon/epoxy laminates. The 494 kA case dramatically exceeds actual worst-case in-service lightning events, and is included for illustration purposes. The SWOs were calculated from classical arc channel expansion theory and arc channel energy balance equations [34]. The dynamic evolution of lightning shock waves involves complex hydrodynamics, plasma physics, and radiative heat transfer. In addition, the magnitude (or strength) of a SWO strongly depends on various arc discharge parameters (*i.e.*, peak current and temporal characteristics of lighting current waveforms). Therefore, it is not straightforward to calculate an accurate value of SWO. In essence, the SWO is related to a release of a massive quantity of electrical (arc) energy. Based upon this, alternatively, one may consider an *equivalent* ABO resulting from shock wave propagation caused by explosions. In contrast to the SWO, all ABO parameters are simply a function of a scaled distance and weight of explosive charge, thus an ABO is relatively easy to implement in numerical models. In this study, ABO and its temporal characteristics were calculated using the amount of chemical potential energy released by explosion equivalent to the lightning's shock wave energy. Trinitrotoluene (TNT) explosions were chosen as a reference baseline.

Background

As described previously, lightning creates an initially cylindrical plasma arc channel. An arc channel radius is associated with lightning waveform parameters; a numerical estimate of a return stroke with 100 kA peak current has an arc channel radius exceeding 5 cm [10]. A substantial amount of Joule heating produced inside an arc channel instantaneously heats and pressurizes the surrounding air. This compresses air inside the arc channel and creates shock waves. Since the expansion velocity of this compressed air is faster than the speed of sound, lightning initiates shock

waves propagating at supersonic velocities. Details concerning SWOs caused by arc channel expansion and equivalent ABOs resulting from TNT explosions are briefly addressed in the following sections.

Shock Wave Overpressures (SWOs)

Lightning transfers a massive electrical energy from “electrically charged clouds" to the neighboring areas [19]. To balance a charge difference between ionized and un-ionized regions, lightning occurs with a local breakdown of the air, which is called *arc channel expansion*. The characteristics of shock front propagation were explicitly investigated for cylindrical shock waves [35] and planar shock waves [36]. These publications [35, 36] define the relationship between shock wave energy and various parameters associated with arc channel expansion. The shock wave energy (E_0) due to an arc channel expansion in high-current impulse arc discharge can be expressed as [34].

$$E_0 = \frac{P_0 B\gamma \left(\frac{2}{n+2}\right)^2 R^n h}{\left[\frac{1}{c}\frac{P_0}{\Delta P}\frac{2\gamma}{\gamma+1}\left(\frac{2}{n+2}\right)^2 + 1\right]^{\left\{2n^2/2n-1\right\}} - 1} \quad (1)$$

Here, P_0 is the ambient pressure; B is a geometry-dependent parameter [37]; γ is the ratio of the specific heat at constant pressure to that at constant volume ($\gamma = 1.4$ for diatomic perfect gases. However, the channel of ionized air is exposed to high temperature and pressure, so using 1.4 for γ is a strong assumption); n represents a type of shock wave (*i.e.*, $n = 1$ for plane shock, $n = 2$ for cylindrical shock, and $n = 3$ for spherical shock), c and h are dimensionless constants defined as a function of n; and ΔP represents the SWO. The derivation of the shock wave energy equation, Eqn. (1), is available in reference [34]. Application of Eqn. (1) assumes self-similar arc expansion (*i.e.*, a cylindrical arc remains cylindrical). In practice, however, the expanding arc cross-section

shape is strongly influenced by the anisotropy in material properties of the target surface at the lightning attachment point [38].

Shock wave theory assumes that arc channel energy is instantaneously released at a point, a line, or a face in the surrounding medium. This assumption is valid for strong shock waves (from detonations), but not for weak shock waves (from transient heat conduction or mass diffusion, *etc.*) due to a time delay in an early stage of shock wave generation [39]. Eqn. (1) shows the shock wave energy is a function of the ambient pressure (P_0) and several dimensionless parameters (*i.e.*, B, γ, n, h, and c). In practice, the shock wave energy is also associated with an arc channel radius, peak current, and rise/decay time durations [9]. These parameters will affect the conversion of arc channel energy (total amount of released energy for arc discharge) to shock wave energy. Such complicating arc discharge parameters are not considered in classical shock wave theory. Xiong *et al*. [34] demonstrated the SWO magnitudes generated by high-current impulse arc discharges having various arc discharge parameters can be also determined from arc channel energy balance equations.

Assuming the shock front expands with the same velocity in the arc channel radial direction, the SWO can be written as

$$\Delta P(t) = K_1 \rho_0 u_1(t)^2 \tag{2}$$

where K_1 is a coefficient of resistance; $K_1 = 2/\gamma + 1$ or $K_1 = 2(\gamma + 1)/(\gamma - 1)^2$ in the stationary or moving reference frames, respectively [40]; ρ_0 is the initial gas density; and $u_1(t)$ refers to the arc channel radial expansion velocity, *i.e.*, the first derivative of the arc channel radius, $r(t)$, with respect to time:

$$r(t) = \left(\frac{108}{125\pi^2 K_1 \rho_0 \sigma_A \xi}\right)^{\{1/6\}} i(t)^{\{1/3\}} t^{\{1/2\}} \tag{3}$$

In Eqn. (3), σ_A is the constant arc channel electrical conductivity, $\xi = (\gamma + 1/6)/(\gamma - 1)$ is a dimensionless coefficient, and $i(t)$ is the time-varying arc discharge current. The corresponding arc channel expansion velocity, $u_1(t)$, [34] is:

$$u_1(t) = \frac{dr(t)}{dt} = \left(\frac{108}{125\pi^2 K_1 \rho_0 \sigma_A \xi}\right)^{\{1/6\}} \left(\frac{i(t)^{\{1/3\}} t^{\{-1/2\}}}{2} + \frac{i(t)^{\{-2/3\}} t^{\{1/2\}}}{3} \frac{di(t)}{dt}\right) \quad (4)$$

Figure 1 displays two overpressure attenuation curves calculated from the arc expansion theory, Eqn. (1), and the energy balance relations, Eqns. (2) and (4), respectively. The SWOs obtained from the arc expansion theory are greater at lower arc channel radii (< 10 mm) and have greater decay rates than those from the energy balance equations. This is due to the assumption in classical shock wave theory that shock waves are fully released at the beginning of arc channel expansion. For each peak current value, the intersection point of two overpressure attenuation curves represents a demarcation point (Fig. 1). This point is defined as a critical arc channel radius at which the arc channel's energy is no longer converted into SWO.

Several tests were performed at high-current impulse arc discharges to calculate the magnitudes of the spark channel energy. This energy represents the total amount of energy released from one electrode to another in a high-power gas switch [34, 35]. Only a fraction of the spark channel energy is converted into shock wave energy. The conversion of spark channel energy to shock wave energy is about 2% when the spark channel energy is less than 0.1 kJ [41]. Furthermore, the conversion rate decreases as the magnitude of spark channel energy increases [34]. A lightning strike is an extremely high impulse discharge current with a few mega-Joules of channel energy. Thus, the shock wave energy is considered to be 1% of the spark channel energy in this study. This conversion ratio is consistent with the work of Xiong *et al*. [34].

Air blast Overpressures (ABOs)

An explosion refers to an extremely rapid, exothermic chemical reaction that releases a large amount of chemical potential energy over few milliseconds. There are two types of explosions: (1) detonation and (2) deflagration. Detonation is a supersonic wave that travels through extreme shock compression of explosives, while deflagration is a subsonic wave that propagates by heat conduction or mass diffusion [42]. The peak overpressure intensity induced by deflagration is much smaller than that by detonation. Lightning creates a cylindrical arc channel and its shock waves propagate at supersonic speeds as high as Mach 10 [43]. Therefore, lightning-induced shock waves may be idealized as those caused by detonations. Similar to lightning, when a detonation occurs, a large amount of chemical potential energy instantaneously heats and pressurizes the surrounding air. The rapid expansion of detonation products creates a hot, dense, high pressure shock wave known as ABO. This propagates radially outward from the center of the explosive source to the surroundings. In this study, ABOs were used to approximate the lightning SWOs. The advantage of using ABO for predicting lightning mechanical damage in composite laminates is due to its easy implementation. While all SWO parameters are associated with complex hydrodynamics and arc channel parameters, those for ABO only depend on a scaled distance and weight of explosive charge, which can be directly calculated from chemical potential energy equivalent to lightning shock wave energy.

The spatial and temporal effects of an explosion's shock wave on a structure depend on (1) structural features (material properties, dimensions, *etc*.), (2) proximity to the explosion center (distance between explosion center to structure), and (3) magnitude of detonation (type, size, weight of charge, *etc*.) [40, 42]. Scaling laws can be used to correlate the effects of proximity to the explosion center and the weight of explosive charge on shock wave generation. All shock wave parameters associated with an ABO can be expressed as a function of a scaled distance and weight

of explosive charge. According to the Hopkinson-Cranz scaling law [45, 46], a scaled distance (Z) is defined as:

$$Z = \frac{R}{W^{1/3}} \tag{5a}$$

where R is the stand-off distance, defined as the distance from the explosion center to the target structure, and W is the weight of explosive charge. For a high explosive (such as TNT), W can be converted into the chemical potential energy (E) by an energy conversion factor (i.e., TNT = 4.184 kJ/g). Thus, Eqn. 5a can be also written as

$$Z = \frac{R}{E^{1/3}} \tag{5b}$$

Figure 2 shows the idealized incident shock front's pressure-time history of a free air blast. The initial shock front pressure is equal to the ambient pressure (P_a). The time required for shock waves to propagate from the explosion center to target structure denotes the arrival time (t_a). Since shock waves propagate at supersonic speeds, shock wave arrival times are very small. As a shock wave encounters a target surface, the incident wave undergoes a pressure jump (an almost instantaneous increase with extremely small rise time) to its maximum value (P_{max}). The difference between the maximum overpressure (P_{max}) and the ambient pressure (P_a) is defined as peak overpressure (P_{io}) or ABO. The shock wave expansion velocity and corresponding overpressure both decrease as time increases. After reaching a peak value at time t_a, the incident shock front pressure decays exponentially back to P_a and is followed by a negative (smaller than P_a) phase. In Fig. 2, the time durations of positive and negative phases are defined as t_o and t_o^-, respectively. A negative phase is usually less important than a positive phase since structural damage induced by an incident air blast mostly occurs in an early stage of shock wave generation [42].

The Friedlander equation [47] is used to mathematically represent the positive phase of an ABO with exponential decay as follows:

$$P_{io}(t) = (P_{so} - P_a)\left(1 - \frac{t - t_a}{t_o}\right)\mathrm{e}^{-\left\{\beta \frac{t-t_a}{t_o}\right\}} \tag{6}$$

where P_{max}, P_a, t_a, and t_o represent the maximum overpressure, the ambient pressure, the arrival time, and the positive time duration, respectively, and β is a dimensionless decay coefficient, which depends on the shock front shape [48] and the stand-off distance [49] that varies nonlinearly with weight of explosive and distance (see Eqn. 5a).

Any structure under a near-field air blast reflects an incident shock wave. A reflected shock wave further compresses forward-moving air molecules. As a result, the reflected overpressure is Mach number dependent and can be 30 times greater than the incident maximum overpressure for Mach = 5 [49].

The magnitude of the reflected overpressure drops as the shock incidence angle (θ) rises. When an incident shock wave travels normal to surface (*i.e.*, $\theta = 0°$), the reflected overpressure and corresponding impulse load (integration of overpressure over time) are at a maximum. If an incident wave propagates at an oblique angle ($0° < \theta < 90°$) to the surface, the reflected peak overpressure decreases, but not monotonically. The minimum reflected overpressure and corresponding impulse results from an incident overpressure at $\theta = 90°$. The reflected overpressure (P_{ro}) is a function of the incident overpressure (P_{io}), and can be written as [50]:

$$P_{ro}(t) = 2P_{io}(t) + (\gamma + 1)\, q(t) \tag{7}$$

where $\gamma = 1.4$ is the ratio of the specific heat of air at constant pressure to that for air at constant volume. The Rankine-Hugoniot conditions [51] can be used to determine the dynamic pressure at the shock front, q(t):

$$q(t) = \frac{P_{io}(t)^2}{2\,\gamma\,P_a + (\gamma - 1)P(t)} \tag{8}$$

The total overpressure (P) acting on structure from both the incident and reflected shock waves can be expressed as a function of P_{io} , P_{ro}, and θ [52]:

$$P(t) = \begin{cases} P_{io}(t)[1 + \cos\theta - 2\cos\theta^2] + P_{ro}(t)\ \cos\theta^2, & \cos\theta \geq 0 \\ P_{io}(t), & \cos\theta < 0 \end{cases} \tag{9}$$

More details on the oblique angle dependence of the incident overpressure (P_{io}), the reflected overpressure (P_{ro}), and the total overpressure (P) are available in [49].

The ABOs and corresponding impulse loads were obtained from the Conventional Weapons Effects Program (CONWEP) [48] developed by the US Army Corps of Engineers. The CONWEP air blast model built into ABAQUS [52] was implemented in the FE models and used to estimate air blast parameters as a function of a scaled distance, Eqn. (5), and the weight of TNT charges. The methods for calculating a scaled distance and weight of TNT charges are discussed in the following sections.

Finite Element Model Development

Implementation of SWOs and equivalent ABOs

The implementation of SWO requires more computational efforts/steps to predict lightning mechanical damage than that required for ABO. Figure 3 compares flow charts for SWO and ABO models implemented in this study. To develop the SWO model, the first step is to calculate a critical arc channel radius from the shock wave energy derived from arc expansion theory, Eqn. (1), and the energy balance relations, Eqns. (2) and (4). The time-varying SWO from the energy balance relations, Eqns. (2) and (4), is associated with a temporally varying current waveform. ABAQUS dynamic analysis is then performed to predict the responses of composite

laminates subjected to SWOs. In contrast, the first step for developing the ABO model is to calculate the spark channel energy from an electrical current action integral (defined as the integral of the square of the electrical current over time). Equivalent TNT mass and a scaled distance are then determined by equating chemical potential energy to the lightning shock wave energy (1% of the spark channel energy in this study). Finally, an ABAQUS built-in CONWEP air blast model is performed to estimate composite structural responses. Note that the SWO is applied over a critical lightning arc channel area, while the equivalent ABO is distributed over entire outermost composite ply surface.

Table 1 includes the SWO and the equivalent ABO parameters for 124, 247, and 494 kA peak current impulse arc discharges. In general, the SWOs roughly scale in proportion with the peak current. Note that the demarcation points (Table 1) are the critical arc channel radii (Fig. 1) that refer to the intersections of the SWO attenuation curves obtained from (1) arc expansion theory and (2) arc channel energy balance equations. The SWOs and demarcation points are proportional to the impulse arc discharge peak currents. This is reasonable because as the peak discharge current becomes higher, more channel energy is released. The equivalent ABOs were calculated from the chemical potential energy released from TNT detonations. The chemical potential energy from TNT is taken as equal to the shock wave energy (1% of the spark channel energy) (Table 1). The explosion of 1 g of TNT releases a chemical potential energy of 4.184 kJ. Using this value, the equivalent TNT mass ("TNT equivalent") can be calculated from the shock wave energy. In the laboratory-scale high-current impulse discharge test apparatus used previously [23–25], custom made two-electrode switches were implemented in the current generators to initiate high impulse currents. Two electrodes faced each other and provided a high current discharge path. The gap spacing between electrodes was a few centimeters [23–25]. A 1 cm distance from the equivalent

TNT explosion center to AS4/3506 carbon/epoxy laminates was used in the FE models. Using this 1 cm gap spacing, a scaled distance can be obtained using Eqn. (5) for each peak current amplitude.

Material properties of AS4/3506 carbon/epoxy laminates

This study compares mechanical damage development in AS4/3506 carbon/epoxy laminates caused by SWOs, which undergo arc channel expansion, and equivalent ABOs from TNT explosions. The orthotropic AS4/3506 plies provide the target with relatively high stiffness and strength in the local fiber direction compared to those in the transverse and thickness directions. This leads to less ply damage in the fiber direction and relatively more damage in other directions. In practice, composite in-plane properties can be tailored by adjusting the ply fiber orientations and stacking sequence. An out-of-plane load (foreign object impact from bird strike, lightning strike, hail, *etc.*) may induce significant matrix damage within plies or local delamination underneath the impact location.

The Hashin failure criteria implemented in ABAQUS [52] are used to predict in-plane damage initiation. This involves (1) fiber damage in tension, (2) fiber damage in compression, (3) matrix damage in tension, and (4) matrix damage in compression. More details on Hashin's four failure criterion are available in reference [53]. Delamination failure from both SWOs and ABOs was not considered in this work. Foster *et al*. [33] predicted delamination initiation of T700/M21 carbon/epoxy laminates under lightning-induced mechanical pressures using cohesive zone modelling. They concluded that delamination failure is relatively minor compared to thermal damage. Delamination failure also may occur and interact with thermal damage. For instance, matrix decomposition in resin-rich areas due to instantaneous Joule heating also can induce delamination failure. Lee *et al*. [18, 19] performed coupled thermal-electrical analyses followed by nonlinear heat transfer analyses to predict epoxy matrix decomposition in AS4/3506

carbon/epoxy laminates subjected to severe lightning strikes. These studies [18, 19] are now being extended to include composite mechanical damage development due to lightning strikes. Table 2 lists the *room* temperature elastic properties and strengths [51, 52] of a typical AS4/3506 carbon/epoxy ply used in these FE models.

Standard current waveform and overpressure-time profiles

The Society of Automotive Engineers (SAE) Aerospace Recommended Practice (ARP) 5412 [56] defines idealized high impulse current waveforms that are consistent with *actual* lightning strikes. Such standard current waveforms and their corresponding parameters (*i.e.*, peak current, time duration, charge transferred, and action integral) depend on the type of lightning strike considered. The SWOs used in the FE models were assumed to have the same temporal characteristics as the standard current waveform A with a 200 kA peak current [56]. Figure 4 shows the temporal variation of current waveform A and corresponding SWO normalized by their respective peak values. The overpressure values between the data points (closed diamonds) are assumed to vary linearly in the FE simulations. Note that the normalized SWO-time profile shown in Fig. 4 is associated with arc channel expansion and arc channel energy balance equations. The ABO-time profiles were calculated from CONWEP air blast models using the scaled distances and the weight of TNT charges (Table 1). These are addressed in the following sections.

FE representation of AS4/3506 carbon/epoxy laminates

The simulated AS4/3506 carbon/epoxy laminates had in-plane 150 mm × 150 mm (length × width) dimensions and a $[45/0/–45/90]_{2S}$ quasi-isotropic layup. The modeled laminate was discretized using 4-node shell elements with reduced integration (S4R element in ABAQUS [52]). A preliminary mesh sensitivity study with element sizes varying from 6 to 1 mm determined

that a maximum element size of 2 mm × 2 mm is required for mesh-independent solutions. Using shell elements to predict in-plane damage in composite plies is computationally more efficient than using multiple solid elements through the thickness since delamination was not considered. As mentioned previously, the goal of this study is to predict in-plane damage initiation/growth that occurs from SWOs and ABOs. Thus, using shell elements dramatically reduced the overall computational time. All four edges of the simulated laminates were encastred (displacements and rotations are completely fixed/clamped), as shown in Fig. 5. The boundary conditions employed in the FE models was motivated by that used in laboratory-scale air blast tests performed by Dharmasena *et al*. [57].

Figure 6 depicts typical FE representations of the simulated AS4/3506 carbon/epoxy laminates subjected to the SWO and equivalent ABO. The areas where the overpressures were applied are highlighted in red. Lightning or a high-current impulse arc discharge produces shock waves propagating along a cylindrical arc channel (Fig. 6a). The local current density and corresponding SWO might be higher near the outer radius of an initial arc channel than in the interior. However, the actual gradients in both the current density and overpressure are not known. The magnitude of lightning-induced SWO decreases exponentially as the distance from the arc channel outer radius increases [32]. This suggests that SWOs applied outside an arc channel may be negligible. Therefore, a uniformly distributed overpressure was only applied within the arc channel radius. The demarcation points (Table 1) were considered initial arc channel radii for the SWOs. Arc channel radii were assumed to be constant during this set of FE simulations. The demarcation points calculated from 124 and 494 kA peak current amplitudes varied from 6.5 to 7.2 mm. The difference in demarcation points (0.7 mm) was smaller than the FE edge length (2 mm). This small difference in the demarcation points (*i.e*., arc channel radii) may not lead to a significant change

in mechanical damage development. Thus, a 6 mm radius arc channel was used in all FE simulations. In contrast to the SWO that is confined within the cylindrical arc channel, ABO creates shock waves propagating radially from the explosion center to an AS4/3506 carbon/epoxy laminate. The outermost composite ply facing the explosion will be strongly influenced by the ABO. The physics of this process was accounted for in the FE simulations, as suggested in Fig. 6b. Note that the scaled distances and the equivalent TNT masses used in the FE models are listed in Table 1.

Results and Discussion

Predicted ABOs and their impulse loads

While the magnitudes (Table 1) and temporal variations (Fig. 4) of the SWOs are known, those for ABOs were calculated from CONWEP air blast models. Using a scaled distance and weight of TNT charge as input parameters (Table 1), CONWEP models were used to calculate the ABOs and other associated parameters as a function of time. Figure 7 shows (a) the ABOs and (b) their corresponding impulse loads predicted at the center of the AS4/3506 carbon/epoxy laminates for 124, 247, and 494 kA peak current impulse arc discharges. When the shock waves propagating from the TNT explosion center reaches the composite, the ABO increases almost immediately from zero to its maximum value. Assuming a zero incident shock front arrival time ($t_a = 0$), the peak incident overpressures occur at $t = 0$. Once the ABOs reach their peak values, they decay exponentially over time. The chemical potential energies of 2.13, 4.26, and 8.51 kJ correspond to arc channel energies from the 124, 247, and 494 kA peak current impulse arc discharges, respectively. These, in turn, produce 1.24, 2.51, and 14.6 MPa peak ABOs and their corresponding 24, 30, and 125 Pa·s peak impulse loads. Clearly, the peak incident ABOs and corresponding impulse loads increase nonlinearly with the peak lightning current. As previously mentioned, a

1cm stand-off distance between the TNT explosion center and the AS4/3506 laminate was used to calculate the scaled distances (Table 1) for each peak lightning current. A *two*-fold increase in the peak current (from 247 kA to 494 kA) resulted in a nearly *six*-fold increase in the peak incident ABO (from 2.51 MPa to 14.6 MPa). The magnitudes of the peak ABOs are smaller than those from the SWOs (Table 1). This is reasonable because the ABO is distributed over the entire composite outer ply surface, while the SWO is only applied within a 6 mm radius arc channel. As a result, the arc channel attachment in a AS4/3506 carbon/epoxy laminate experiences more intense local compressive loads from the SWO.

Predicted midplane displacement

In this work, the SWOs and ABOs each struck the laminated composite surface at the same time, *i.e.*, shock wave arrival time ($t_a = 0$). Material and geometrically nonlinear transient ABAQUS FE analyses were performed to predict mechanical damage development in quasi-isotropic AS4/3506 flat laminates subjected to normal incident overpressures at their geometric center on the outermost ply (Fig. 6). Three sets of SWOs and ABOs were considered, each corresponding to 124, 247, and 494 kA peak lightning current. Figures 8a-8d contain plots of the transverse midplane displacements evaluated at the laminate geometric center, a point 10 mm above the center, a point 10 mm to the right of the center, and the point 10 mm above and to the right of the center, respectively, due to the SWOs and their corresponding ABOs. In general, the magnitudes of the peak displacements due to each overpressure were comparable, but the SWO displacements (dashed lines) tended to slightly lag the ABO displacements (solid lines). This makes sense since, if $t_a = 0$, the SWO acts like a point source at the center of the panel, whereas the ABO is applied over the entire laminate surface. The relative phase difference in the midplane displacements between the SWO and the ABO is 5×10^{-5} s. Moreover, temporal variations in the

out-of-plane strain rates of AS4/3506 laminates for each peak current amplitude predicted by the SWOs and their equivalent ABOs, evaluated at the laminate geometric center, were also comparable as shown in Figure 9. These suggest that the dynamic responses of a given plate due to each overpressure are quite similar to each other. The peak midplane displacements increased substantially with increasing peak lightning current. Large scale transient flexural vibrations about the laminate midplane due to the initial overpressures and stress wave transmission/reflection cause rapid fluctuations between in-plane tension and compression in each ply.

Figures 10a and 10b show the spatial variations in the peak compressive and tensile midplane displacements evaluated along a horizontal line passing through the laminate center for 124, 247, and 494 kA peak currents. The dotted and solid lines each correspond to the displacements predicted for the SWOs and the ABOs; the small differences in the peak midplane displacements for both predictions increased slightly as the peak current increased. Both the compressive and tensile displacements were maximum at the center ($x = 0$) and had similar distributions. This suggests that the innermost ply also experiences similar combined dynamic tension/compression displacement time histories as does the outermost (impacted) ply. Hence, mechanical damage formation in the both plies should be similar and mechanical fiber/matrix damage may be relatively symmetric about the laminate midplane. In contrast, thermal damage due to lightning strike tends to be unsymmetric about the laminate midplane and concentrated in the outermost plies near the lightning arc attachment point [18–20]. Figure 11 displays a cross-sectional observation of a 32-ply IM600/133 carbon/epoxy laminate after a 40 kA peak lightning strike test. Severe fiber rupture and tow splitting occurring from a rapid temperature increase (*i.e.*, thermal damage) are mostly confined in the first (outermost) or second composite plies, but there is no obvious visible damage to the innermost plies [17–26]. This confirms that lightning thermal damage develops

unsymmetrically about the laminate midplane. Moreover, the evolution of thermal damage can be combined with the evolution of mechanical damage during and after lightning strike. An investigation of mechanically and thermally induced delamination due to lightning will be part of a future investigation.

Mechanical damage prediction using the Hashin's damage criteria

Hashin's damage criteria [53] were used to predict initial fiber failure in tension or compression and matrix failure in tension or compression. Overpressure-induced ply delamination is not considered here, but will be addressed as part of a future study. Lee *et al*. [18, 19] investigated lightning-induced *thermal* damage in AS4/3506 laminates. Lightning thermal damage is generally more widespread and severe than mechanical damage [13, 31]. Nonetheless, overpressure-induced damage, if present, may have an effect on the composite residual strength after lightning strike. The overarching goal of our research is to predict coupled mechanical and thermal lightning damage development in carbon-epoxy laminates that accounts simultaneously for strain rate and temperature-dependent material properties, localized Joule heating, transient heat transfer, and stress/shock wave propagation. This current work aimed at mechanical damage initiation is an important step in that process.

If any Hashin failure index equals or exceeds the unity (≥ 1) during loading, damage then initiates [53]. Figure 12 shows Hashin's four failure index distributions in the top AS4/3506 carbon/epoxy ply subjected to a 22 MPa SWO and the equivalent ABO determined from 2.13 kJ of chemical potential energy; these two overpressures are equivalent to the mechanical pressure induced by a 124 kA peak current. Figures 12a-12d show the predicted Hashin failure index distributions due to SWO and ABO for fiber compression, fiber tension, matrix compression, and matrix tensile failures, respectively. In each case, the peak value of the failure index was well

below 1 (<0.1), *i.e.*, fiber and/or matrix failure was not close to being imminent for the 124 kA strike. Use of either SWO or ABO led to failure index distributions with the same essential character and magnitudes. The predicted failure indices in the top ply are slightly greater when subjected to the SWO than ABO. This makes sense because the SWO is relatively localized, acting at the arc channel attachment location and causing higher failure indices at and around this region. The peak SWO matrix tension failure value is somewhat higher than that for ABO at the arc attachment due to damage localization in the smaller area mentioned above.

For all SWO and ABO damage modes corresponding to a 124 kA peak current, the magnitudes of all four damage indices are much less than unity, so no damage initiation is predicted. These FE results show that the mechanical pressure loading calculated from a high current impulse lightning discharge (124kA peak current) is unlikely to create noticeable damage in AS4/3506 carbon/epoxy laminates. In contrast, lightning strike experiments performed by Hirano *et al.* [23] (for IM600/133 carbon/epoxy laminates), by Feraboli *et al.* [25] (for HTA/7714A carbon/epoxy laminates), and by Lacy *et al.* [28,29] (for AS4/VRM-34 warp-knitted carbon/epoxy fabrics), and lightning thermal damage prediction models developed by Lee *et al*. [18–20, 58] for AS4/3506 carbon/epoxy laminates suggested that significant matrix decomposition (thermal damage) occurs from 40 kA peak current strikes. Hence, thermal damage development due to lightning strike is generally considered to be a bigger concern than mechanical damage.

Since no mechanical damage initiation was predicted from a 124 kA peak current, the peak current of the impulse discharge was nearly doubled to 247 kA (Fig. 13). At this current, all damage failure indices only slightly increased, but all were still lower than 0.3, indicating mechanical damage formation was not imminent. Both the SWO and equivalent ABO gave similar predicted Hashin fiber and matrix damage mode indices in the top AS4/3506 carbon/epoxy ply.

The encastred boundary conditions constrain displacement and rotation of the elements at the edges, leading to slight stress concentrations (and locally higher Hashin indices) as each laminate is forced to bend over the rigid support. This slightly higher stress concentration at the edges is noticeable in the fiber tension failure index distribution (Fig. 13b). In practice, a 200 kA peak current lightning strike is considered an extreme outlier and upper bound on expected naturally occurring strikes [56]. The numerical simulations performed using a 247 kA peak current suggest that composite fiber and matrix damage is unlikely in the vicinity of the attachment point. Based upon the relative magnitudes of the Hashin failure indices, matrix failures are likely to initiate well before fiber failure as the current is increased.

For illustration purposes, an additional set of mechanical damage analyses were performed using a peak current of 494 kA. The SWO (and equivalent ABO) due to such an extreme current is unlikely to occur due to actual lightning, but may have implications in high-energy weapons applications. Figure 14 shows Hashin's four failure index distributions in the top AS4/3506 carbon/epoxy ply subjected to a 69 MPa SWO and its equivalent ABO determined from 8.51 kJ, equivalent to the 494 kA peak current. Application of either SWO or ABO or these magnitudes led to overall distributions of the Hashin failure indices in the top AS4/3506 carbon/epoxy ply shown in Figure 14. Similar to the analyses performed at 124 kA (Fig. 12) and 247 kA (Fig. 13) peak currents, fiber tensile and compression failures were not imminent (failure indices ≤ 0.8), with the exception of matrix tension failure (Fig. 14d). For the SWO and ABO associated with the 494 kA peak current, initiation of matrix tension failure was predicted near the center of the panels. As mentioned previously, the failure index distributions were fairly symmetric about the laminate midplane. This suggests that, with the exception of matrix tension failure predicted at the extreme 494 kA peak current, purely mechanical damage initiation (with the possible exception of

delamination) should not be a major concern for the majority of naturally occurring lightning strikes. Moreover, use of either SWO or *equivalent* ABO led to similar distribution of failure indices in each ply. This implies that these two overpressures may be interchangeably used for characterizing lightning-induced mechanical damage.

An additional set of numerical simulations was performed to compare lightning mechanical damage with corresponding thermal damage in 150 mm × 100 mm (length × width) AS4/3506 carbon/epoxy laminates with a quasi-isotropic layup of $[45/0/–45/90]_{4s}$. Since matrix tension is the most likely mechanical failure mechanism (Figs. 12-14), only the outermost ply matrix tension failure index distribution was compared with the predicted and observed regions with lightning induced matrix thermal decomposition. For a 40 kA peak current lightning strike, Fig. 15a shows the predicted Hashin matrix tension failure index distribution, predicted matrix thermal decomposition from Lee *et al.* [19], and a through-transmission-ultrasonic (TTU) C-scan image of lightning damage from Hirano *et al*. [23]. Consistent with our earlier calculations, no mechanical damage initiation (failure index << 1) was predicted. In contrast, a substantial amount of matrix thermal decomposition was predicted (center image) [19] that correlated very well with experimental observations of damage from [23]. Figure 15b contains analogous predictions of mechanical and thermal matrix decomposition for a 124 kA peak current lightning strike. Again, these results suggests that mechanical damage initiation due to SWO associated with extreme lightning strikes is relatively minor in comparison with composite thermal damage.

Additional studies that improve the lightning or explosion-induced mechanical damage prediction models are ongoing. When a chemical explosion occurs, a fraction of chemical potential energy is converted to thermal energy, which causes a rapid temperature rise at the outer surface of a structure, along with SWO/ABO. The effect of thermo-mechanical coupling on corresponding

composite damage development remains unclear. A fully coupled thermo-electro-mechanical model is being developed for predicting composite damage (including delamination) that accounts for transient dynamic loading, Joule heating, temperature and rate-dependent material properties, and other factors necessary for composite material characterization in extreme environments. In addition, SWOs and ABOs are being defined for high-current impulse waveforms with higher peak currents (up to 500 kA) and different temporal characteristics [34, 35] than standard lightning current waveforms [56].

Concluding Remarks

This work proposes a new approach for predicting lightning mechanical damage using shock wave overpressure (SWO) and its equivalent air blast overpressure (ABO). The simulated 16-ply quasi-isotropic, $[45/0/–45/90]_{2S}$, AS4/3506 carbon/epoxy composites were subjected to the SWOs and the ABOs consistent with 124, 247, and 494 kA peak lightning currents. Dynamic responses of the composite laminates due to both SWOs or equivalent ABOs were quite similar to each other. Both the compressive and tensile displacements were maximum at the center and had similar distributions suggesting that the innermost ply also experiences similar combined dynamic tension/compression displacement time histories. The spatial variations in the peak compressive and tensile midplane displacements evaluated near the center of a composite laminate showed that lightning mechanical damage tends to be symmetric about the laminate midplane, while lightning thermal damage is somewhat unsymmetric about the laminate midplane and mostly concentrated in the outermost plies near the lightning arc attachment point. The predicted Hashin fiber compression, fiber tension, matrix compression, and matrix tension failure indices showed that use of either SWO or ABO led to failure index distributions with the same essential character and

magnitudes. While matrix tension failure was predicted at the extreme 494 kA peak current, purely mechanical damage initiation is not a major concern for the majority of naturally occurring lightning strikes. In conclusion, this study suggests that (1) lightning SWO does not cause significant *mechanical* damage to AS4/3506 carbon/epoxy laminates and (2) it may be possible to interchangeably use either SWO or ABO to predict lightning mechanical damage.

Acknowledgement

This work was not funded by external bodies. The authors appreciate the access to the computational resources provided by the Advanced Composites Collaboration for Innovation and Science (ACCIS) at the University of Bristol.

References

[1] Baker Dutton, S., and Kelly, D. A. Composite Materials for Aircraft Structures. AIAA; 2004.

[2] US Government Accountability Office. Status of FAA's Actions to Oversee the Safety of Composite Airplanes. Aviation Safety 2011.

[3] Pora J. Composite Materials in the Airbus A380 - From History to Future -. Proceedings ICCM-13 2001:1–10.

[4] Gellard G. A380 Composite in Airbus, Global Investor Forum 2008.

[5] Brosius D. Boeing 787 Update: Approaching Rollout and First Flight, the 787 Relies on Innovations in Composite Materials and Processes to Hit its Targets. High Performance Composites 2007;15:56.

[6] Plumer JA, Hourihan BI. Data from the Airlines Lightning Strike Reporting Project. In Proceedings of the Lightning and Static Electricity Conference, 1972.

[7] Fisher FA, Plumer JA, Perala RA. Lightning Protection of Aircraft 1977.

[8] McDowall RL, Plumer JA, Glynn MS, McDowall Plumer, J.A., and Glynn, M.S. RL. Lightning Data Acquisition. Proceedings of the 15th International Aerospace and Ground Conference on Lightning and Static Electricit, Atlantic City, NJ: 1992.

[9] Rakov VA, Uman MA. Lightning: Physics and Effects. Cambridge University Press; 2003.

[10] Thottappillil R, Uman MA. Comparison of Lightning Return-Stroke Models. Journal of Geophysical Research: Atmospheres 1993;98:22903–14. doi:10.1029/93JD02185.

[11] Uman MA, Rakov VA. The Interaction of Lightning with Airborne Vehicles. Progress in Aerospace Sciences 2003;39:61–81. doi:10.1016/S0376-0421(02)00051-9.

[12] O'Loughlin JB, Skinner SR. General Aviation Lightning Strike Report and Protection Level Study. DOT/FAA/AR-04/13, FAA; 2004.

[13] Chemartin L, Lalande P, Peyrou B, Chazottes A, Elias PQ, Delalondre C, et al. Direct Effects of Lightning on Aircraft Structure : Analysis of the Thermal , Electrical and Mechanical Constraints. Journal Aerospace Lab 2012:1–15.

[14] Ogasawara T, Hirano Y, Yoshimura A. Coupled Thermal-Electrical Analysis for Carbon Fiber/Epoxy Composites Exposed to Simulated Lightning Current. Composites Part A: Applied Science and Manufacturing 2010;41:973–81. doi:10.1016/j.compositesa.2010.04.001.

[15] Abdelal G, Murphy A. Nonlinear Numerical Modelling of Lightning Strike Effect on Composite Panels with Temperature Dependent Material Properties. Composite Structures 2014;109:268–78. doi:10.1016/j.compstruct.2013.11.007.

[16] Dong Q, Guo Y, Sun X, Jia Y. Coupled Electrical-Thermal-Pyrolytic Analysis of Carbon Fiber/Epoxy Composites Subjected to Lightning Strike. Polymer 2015;56:385–94. doi:10.1016/j.polymer.2014.11.029.

[17] Wang FS, Ji YY, Yu XS, Chen H, Yue ZF. Ablation Damage Assessment of Aircraft Carbon Fiber/Epoxy Composite and its Protection Structures Suffered from Lightning Strike. Composite Structures 2016;145:226–41.

[18] Lee J, Lacy TE, Pittman Jr. CU, Mazzola MS. Thermal Response of Carbon Fiber Epoxy Laminates with Metallic and Nonmetallic Protection Layers to Simulated Lightning Currents. Polymer Composites 2017;39:2149–66. doi:10.1002/pc.24502.

[19] Lee J, Lacy TE, Pittman Jr. CU, Mazzola MS. Temperature-Dependent Thermal

Decomposition of Carbon/Epoxy Laminates Subjected to Simulated Lightning Currents. Polymer Composites 2017;39:2185–98. doi:10.1002/pc.24535.
[20] Lee J, Lacy Jr TE, Pittman CU, Mazzola MS. Comparison of lightning protection performance of carbon/epoxy laminates with a non-metallic outer layer. Journal of Reinforced Plastics and Composites 2019;38:301–13. doi:10.1177/0731684418817144.
[21] Guo Y, Dong Q, Chen J, Yao X, Yi X, Jia Y. Comparison Between Temperature and Pyrolysis Dependent Models to Evaluate the Lightning Strike Damage of Carbon Fiber Composite Laminates. Composites Part A: Applied Science and Manufacturing 2017;97:10–8. doi:10.1016/j.compositesa.2017.02.022.
[22] Wang Y. Modeling of Lightning-Induced Thermal Ablation Damage in Anisotropic Composite Materials and its Application to Wind Turbine Blades 2016.
[23] Hirano Y, Katsumata S, Iwahori Y, Todoroki A. Artificial Lightning Testing on Graphite/Epoxy Composite Laminate. Composites Part A: Applied Science and Manufacturing 2010;41:1461–70. doi:10.1016/j.compositesa.2010.06.008.
[24] Feraboli P, Miller M. Damage Resistance and Tolerance of Carbon/Epoxy Composite Coupons Subjected to Simulated Lightning Strike. Composites Part A: Applied Science and Manufacturing 2009;40:954–67. doi:10.1016/j.compositesa.2009.04.025.
[25] Feraboli P, Kawakami H. Damage of Carbon/Epoxy Composite Plates Subjected to Mechanical Impact and Simulated Lightning. Journal of Aircraft 2010;47:999–1012. doi:10.2514/1.46486.
[26] Yin JJ, Chang F, Li SL, Yao XL, Sun JR, Xiao Y. Experimental and Numerical Simulation Analysis of Typical Carbon Woven Fabric/Epoxy Laminates Subjected to Lightning Strike. Applied Composite Materials 2017;24:1353–72. doi:10.1007/s10443-017-9588-6.
[27] Wolfrum J, Schuster TJ, Körwien T. Effects of Heavy Lightning Strikes on Pristine and Repaired Carbon Composite Structures. Journal of Composite Materials 2017;51:3491–504. doi:10.1177/0021998317690445.
[28] Lacy TE, Mazzola MS, Kluss J, Boushab D, Gharghabi P, Lee J, et al. Resin Infused Stitched Composite Development: Lightning Strike Testing of PRSEUS Panels. Technical Report for Boeing Purchase Contract 118469 2016.
[29] Lacy Jr. TE, Mazzola MS, Kluss J, Boushab D, Gharghabi P, Lee J, et al. Resin Infused Stitched Composite Development: Lightning Strike Testing of PRSEUS Panels. Technical Report for Boeing Purchase Contract 118469; 2017.
[30] Katunin A, Krukiewicz K, Turczyn R, Sul P, Bilewicz M. Electrically Conductive Carbon Fibre-Reinforced Composite for Aircraft Lightning Strike Protection. IOP Conference Series: Materials Science and Engineering 2017;201:012008. doi:10.1088/1757-899X/201/1/012008.
[31] Reid GW. Mechanical Damage to Aircraft Structures from Lightning Strikes. Proceedings of the Institution of Mechanical Engineers., vol. 68, 2005, p. 44–6, 48–9; quiz 50.
[32] Muñoz R, Delgado S, González C, López-Romano B, Wang D-Y, LLorca J. Modeling Lightning Impact Thermo-Mechanical Damage on Composite Materials. Applied Composite Materials 2014;21:149–64. doi:10.1007/s10443-013-9377-9.
[33] Foster P, Abdelal G, Murphy A. Quantifying the Influence of Lightning Strike Pressure Loading on Composite Specimen Damage. Applied Composite Materials 2018:1–23. doi:10.1007/s10443-018-9685-1.
[34] Xiong J, Li L, Dai H, Wu H, Peng M, Lin F. The Development of Shock Wave

Overpressure Driven by Channel Expansion of High Current Impulse Discharge Arc. Physics of Plasmas 2018;25:032115. doi:10.1063/1.5013296.
[35] Plooster MN. Shock Waves from Line Sources. Numerical Solutions and Experimental Measurements. Physics of Fluids 1970;13:2665. doi:10.1063/1.1692848.
[36] Jones DL. Comments on "Electrically Driven Blast Waves." Citation: The Physics of Fluids 1970;13:1422. doi:10.1063/1.1693092.
[37] Jones DL. The Energy Parameter B For Strong Blast Waves 1962.
[38] Sousa Martins R. Experimental and Theoretical Studies of Lightning Arcs and Their Interaction with Aeronautical Materials. n.d.
[39] Dabora EK. Variable Energy Blast Waves. AIAA Journal 1972;10:1384–6. doi:10.2514/3.6635.
[40] Engel TG, Kristiansen M, Krompholz H. Expansion of Hydrogen Arcs Driven by Oscillating Currents. IEEE Transactions on Plasma Science 1991;19:959–67. doi:10.1109/27.108440.
[41] Liu Q, Zhang Y. Shock Wave Generated by High-Energy Electric Spark Discharge. Journal of Applied Physics 2014;116:153302. doi:10.1063/1.4898141.
[42] Bulson PS. Explosive Loading of Engineering Structures : A History of Research and A Review of Recent Developments. E & FN Spon; 1997.
[43] Few Jr. AA. Acoustic Radiations from Lightning. CRC Handbook of Atmospheres, Boca Raton, FL: CRC Press; 1982, p. 287–90.
[44] Karlos V, Solomos G, Viaccoz B, European Commission. Joint Research Centre. Institute for the Protection and the Security of the Citizen. Calculation of Blast Loads for Application to Structural Components. Publications Office; 2013.
[45] Hopkinson B. British Ordnance Board Minutes. London, UK: 1915.
[46] Cranz C. LEHRBUCH DER BALLISTI. Berlin, Germany: Springer; 1926.
[47] Friedlander FG. The Diffraction of Sound Pulses. I. Diffraction by a Semi-Infinite Plane. Proceedings of the Royal Society A: Mathematical, Physical and Engineering Sciences 1946;186:322–44. doi:10.1098/rspa.1946.0046.
[48] Hyde DW. CONWEP: Conventional Weapons Effects Program. US Army Engineer Waterways Experiment Station. Vicksburg, MS: 1991.
[49] Department of Defense. Structures to Resist the Effects of Accidental Explosions (UFC 3-340-02). Washington DC: 2008.
[50] Dolce F. Blast Impact Simulation on Composite Military Armours. University of Bath, 2009.
[51] Kennel CF, Blandford RD, Coppi P. MHD Intermediate Shock Discontinuities. Part 1. Rankine-Hugoniot Conditions. Journal of Plasma Physics 1989;42:299. doi:10.1017/S0022377800014379.
[52] ABAQUS. ABAQUS Documentation. Dassault Systémes Simulia Corp 2014.
[53] Hashin Z. Failure Criteria for Unidirectional Fiber Composites. Journal of Applied Mechanics 1980;47:329. doi:10.1115/1.3153664.
[54] Michopoulos JG, Hermanson JG, Lliopoulos A, Lambrakos S, Furukawa T. On the Constitutive Response Characterization for Composite Materials Via Data-Driven Design Optimization. In: Proceedings of the ASME 2011 International Design Engineering Technical Conference & Computers and Information in Engineering Conference, August 29-31, 2011 Washington, DC, IDETC/CIE 2011; 13 P 2011:1–13.
[55] Daniel IM, Ishai O. Engineering Mechanics of Composite Materials. Oxford University

Press; 2006.
[56] SAE International. ARP5412B: Aircraft Lightning Environment and Related Test Waveforms. Aerospace Recommended Practice 2013:63.
[57] Dharmasena KP, Wadley HNG, Xue Z, Hutchinson JW. Mechanical Response of Metallic Honeycomb Sandwich Panel Structures to High-Intensity Dynamic Loading. International Journal of Impact Engineering 2008;35:1063–74. doi:10.1016/j.ijimpeng.2007.06.008.
[58] Lee J, Lacy TE, Pittman Jr. CU, Mazzola MS. Thermal Response to Simulated Lightning Currents on Stitched Composite Aircraft Structures. Proceedings of the American Society for Composites: 31st Technical Conference, Williamsburg, VA, Sep 19-21, 2016.

Table 1. Shock wave overpressure (SWO) and equivalent air blast overpressure (ABO) parameters used in the FE analysis

Peak current (kA)	SWO			ABO	
	Channel energy (kJ)	Shock wave Overpressure (MPa)	Demarcation point (mm)	Equivalent TNT mass (kg)	Scaled distance ($m/kg^{1/3}$)
124	2.13	22	6.5	0.0005	0.1252
247	4.26	38	6.8	0.0010	0.0994
494	8.51	69	7.2	0.0020	0.0789

Table 2. Room temperature elastic properties and strengths of AS4/3506 carbon/epoxy ply [54,55]

Elastic properties [54]								
E_{11} (GPa)	E_{22} (GPa)	E_{33} (GPa)	G_{12} (GPa)	G_{13} (GPa)	G_{23} (GPa)	ν_{12}	ν_{13}	ν_{23}
142.5	9.8	9.8	6.279	6.279	3.753	0.29	0.29	0.30
Strengths [55]								
X_T (MPa)	X_C (MPa)	Y_T (MPa)	Y_C (MPa)	S_L (MPa)	S_T (MPa)			
2280	1440	57	228	71	71			

E_{11} is elastic modulus in the longitudinal (fiber) direction; E_{22} and E_{33} are elastic moduli in two transverse directions; G_{12}, G_{13}, G_{23} are shear moduli applied in the 12, 13, 23 directions, respectively; X_T and X_C are tensile and compressive strengths in longitudinal direction; Y_T and Y_C are tensile and compressive strengths in the transverse (perpendicular to fiber) directions; S_L and $S_T$are each indicate shear strengths in the longitudinal and transverse directions.

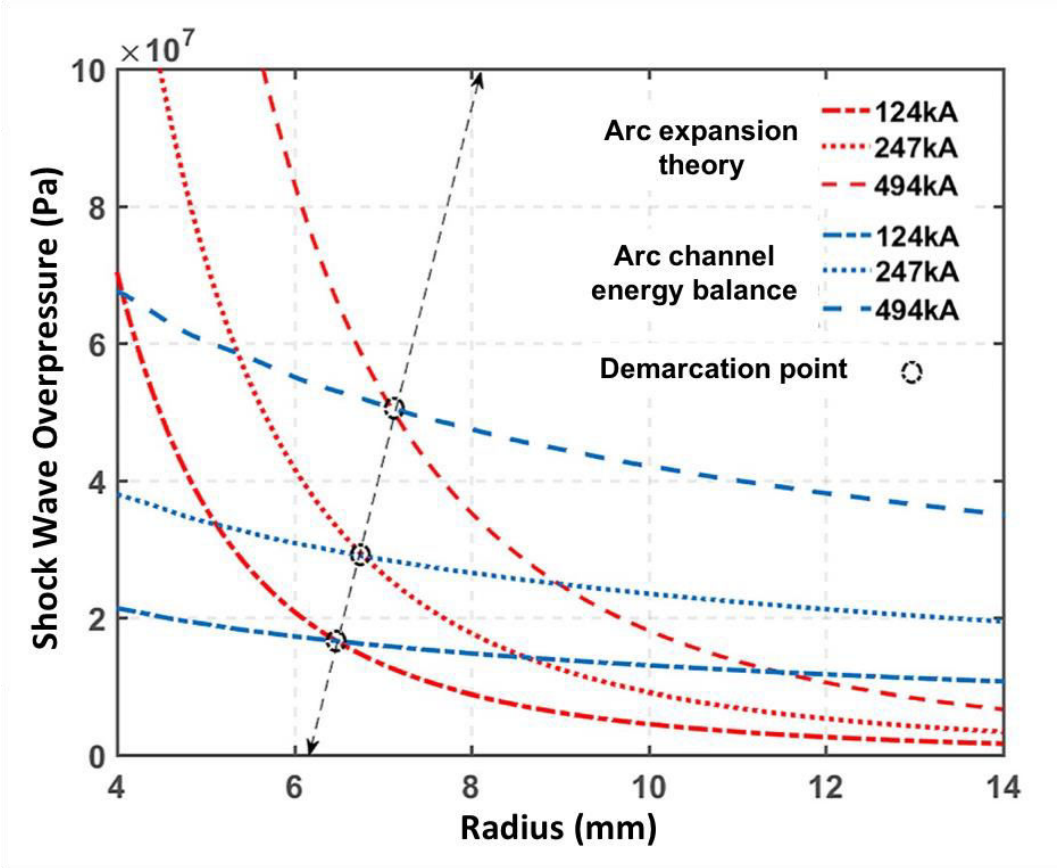

Figure 1. SWO (ΔP) versus an arc channel radius (R) plots of 124, 247, and 494 kA impulse discharge currents (adopted from [34]).

5

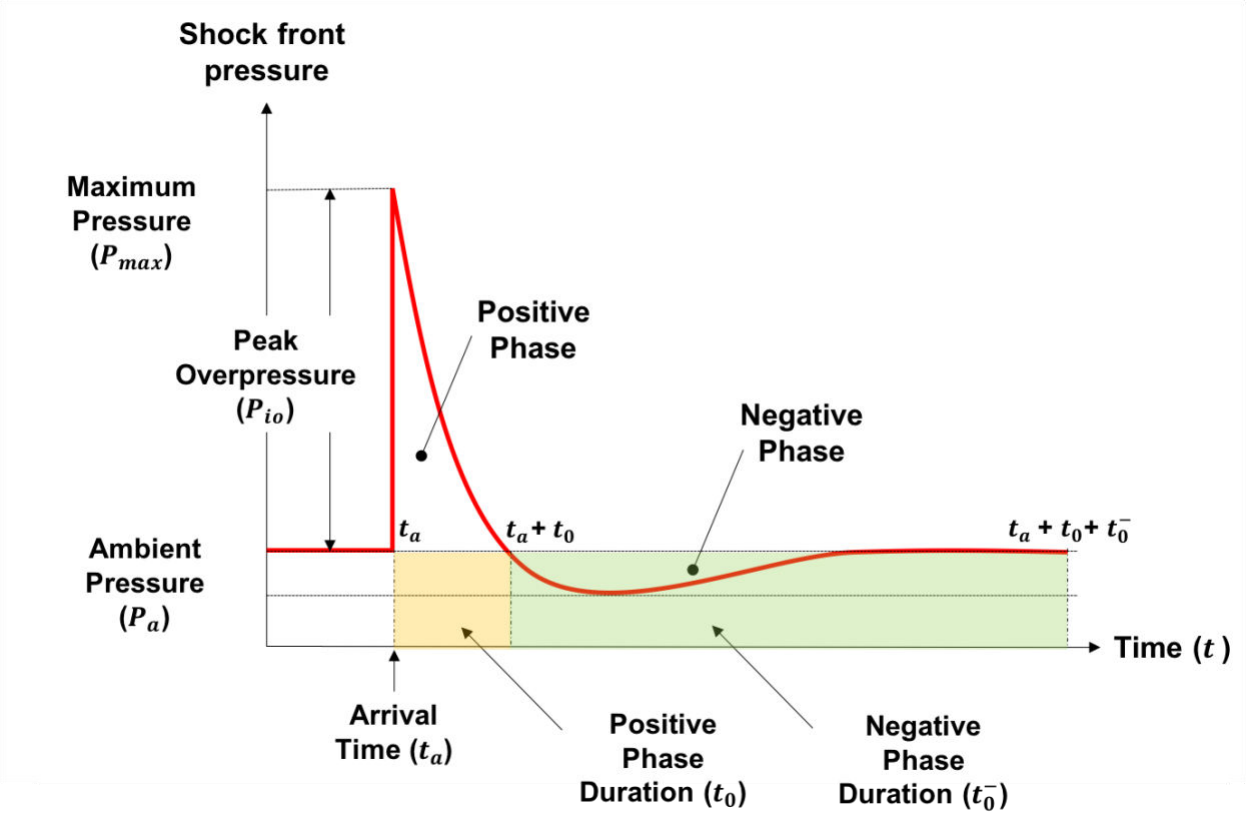

Figure 2. Idealized shock front pressure-time curve for a free air blast.

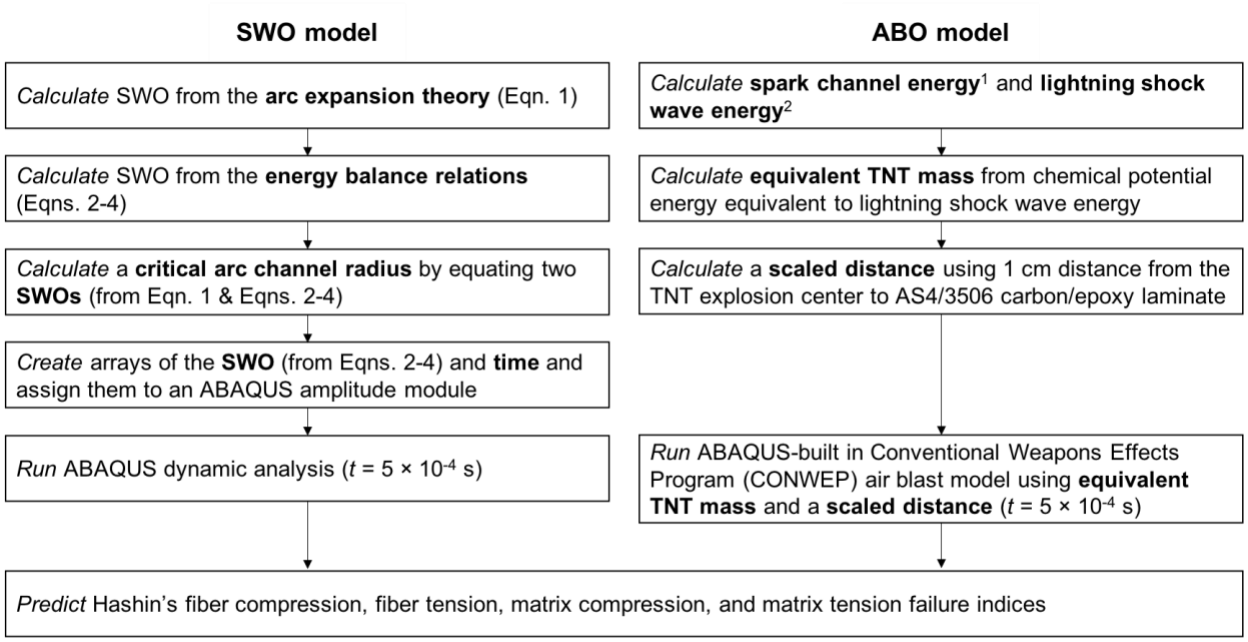

Figure 3. Flow charts for the SWO and equivalent ABO models implemented in this study.

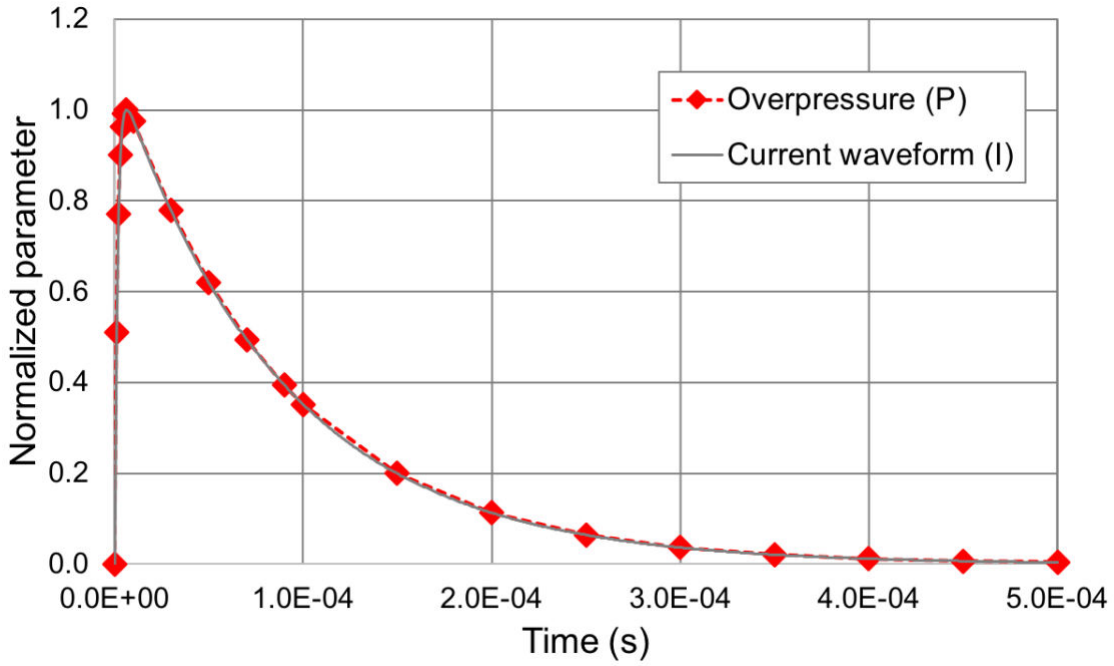

Figure 4. Standard current waveform A (I) and SWO (P) versus time curve normalized by their peak values (I_{peak} = 200 kA from [56] and values from Table 2).

5

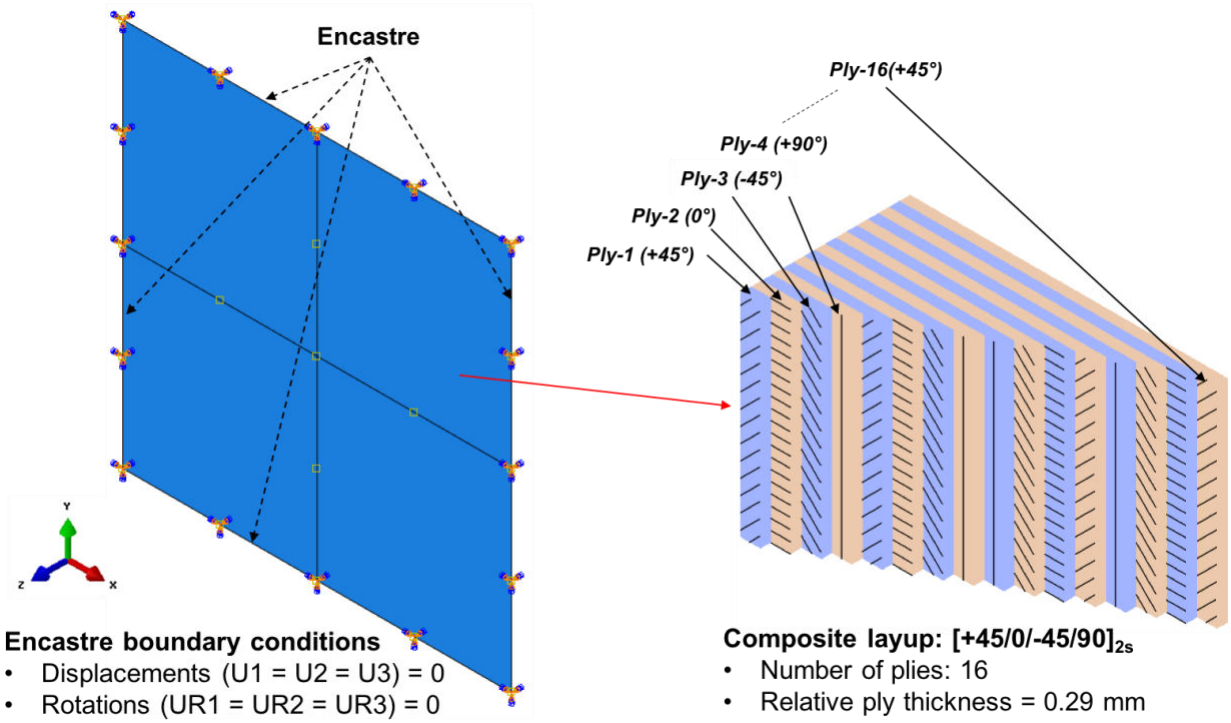

Figure 5. Boundary conditions and layup used in the current FE analysis.

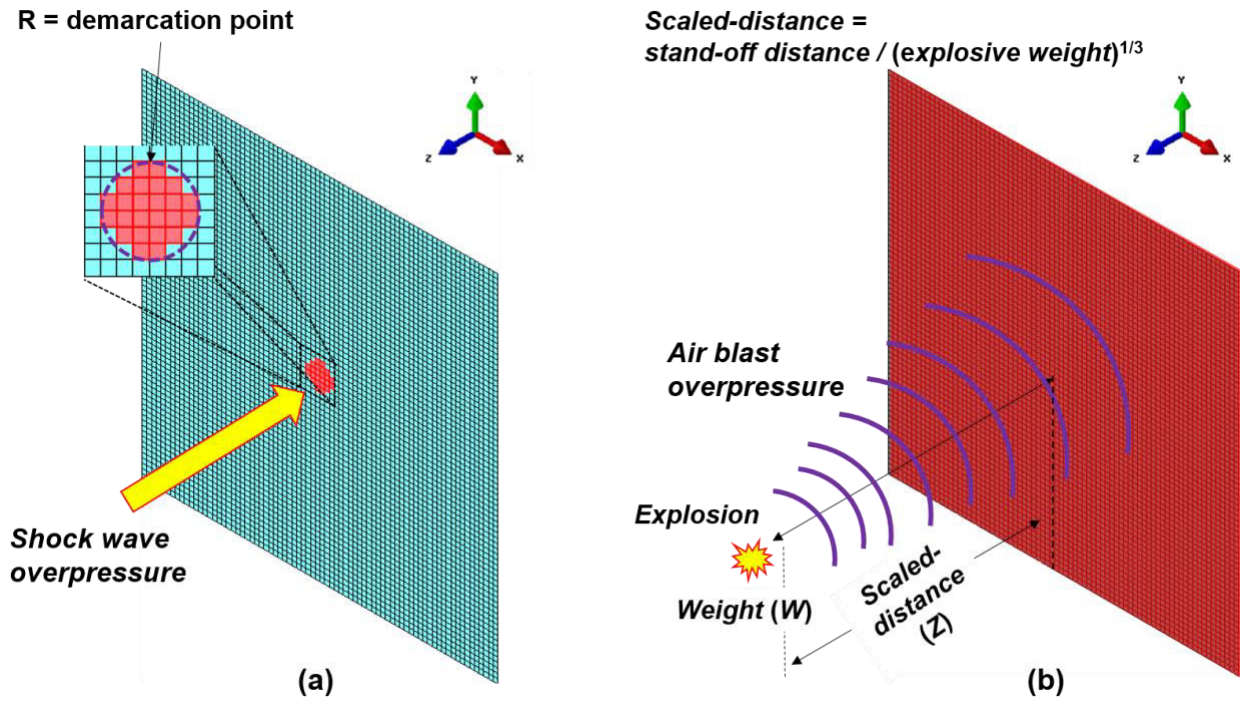

Figure 6. FE representations of (a) SWO model and (b) ABO model. The demarcation points for each SWO and scaled distances (as well as TNT charges) used for each ABO are listed in Table 1. The areas highlighted in red refer to those where overpressures are applied.

5

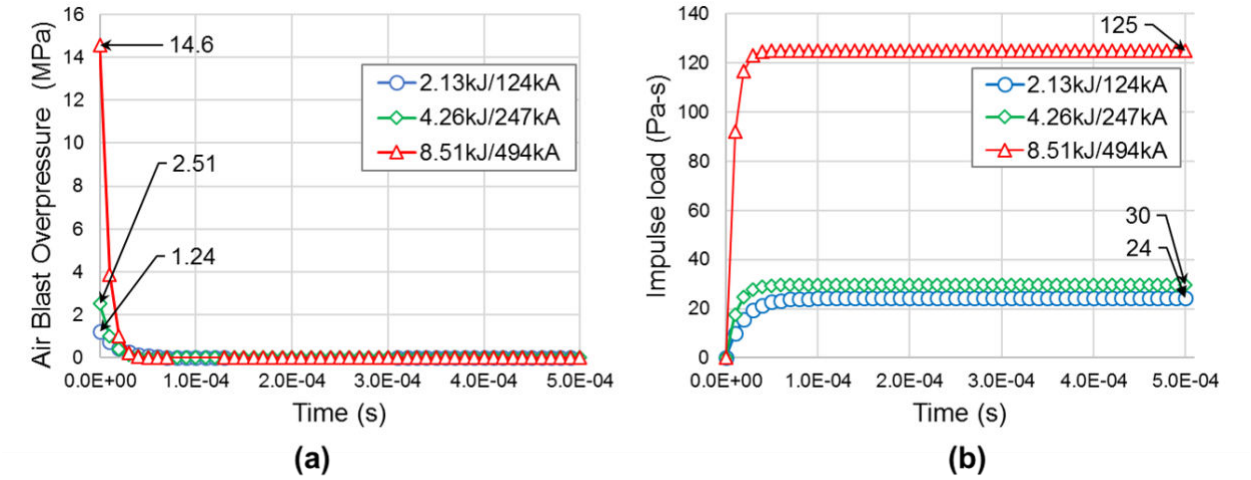

Figure 7. (a) ABOs and (b) their impulse loads at the center of AS4/3506 carbon/epoxy laminates predicted in ABAQUS built-in CONWEP models.

5

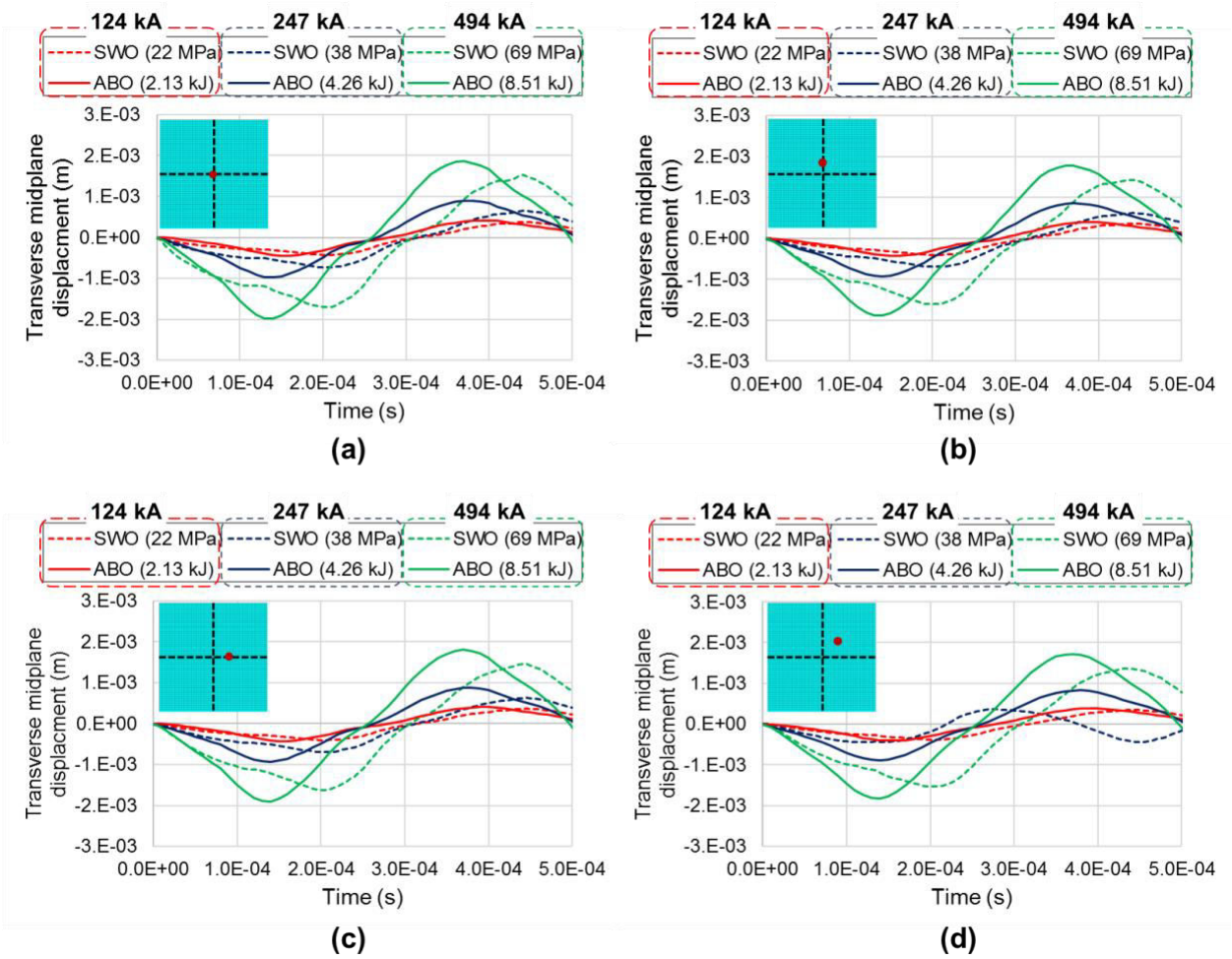

Figure 8. Transverse midplane displacements of AS4/3506 laminates with different peak current amplitudes (Table 1) predicted by the SWOs (dotted lines) and their equivalent ABOs (solid lines) evaluated at (a) the center, (b) the point 10 mm above the center, (c) the point 10 mm to the right of the center, and (d) the point 10 mm above and to the right of the center.

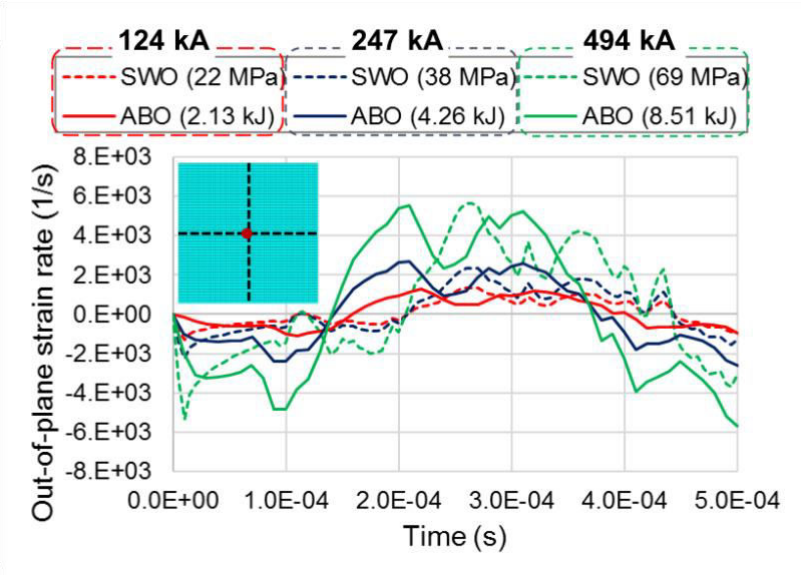

Figure 9. Temporal variations in the out-of-plane strain rates of AS4/3506 laminates for each peak current amplitude (Table 1) predicted by the SWOs (dotted lines) and their equivalent ABOs (solid lines) evaluated at the laminate center.

5

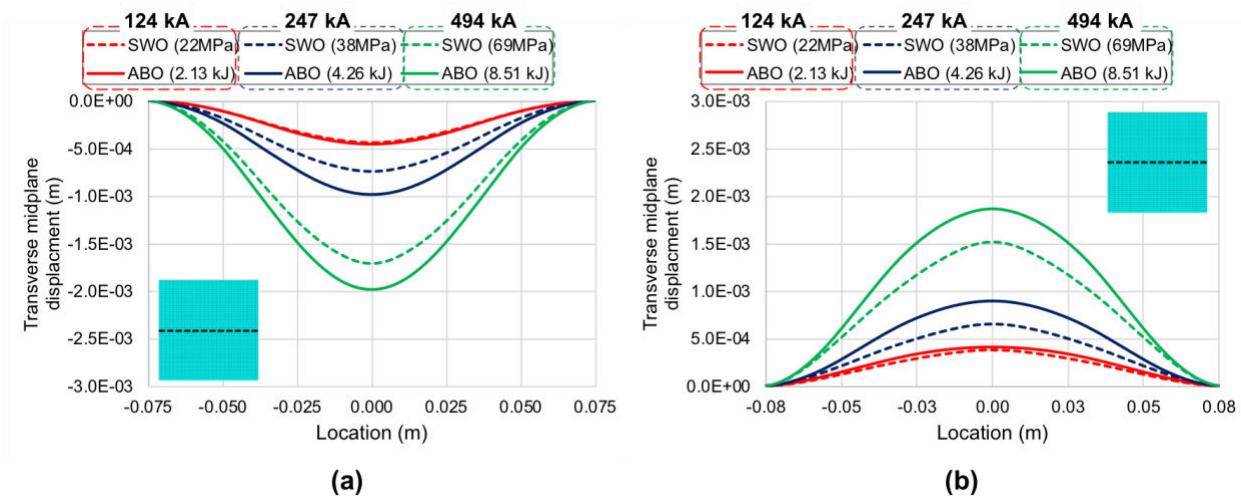

Figure 10. Spatial variations in peak compressive and tensile midplane displacements evaluated along a horizonal line passing through the laminate center for 124, 247, and 494 kA peak currents.

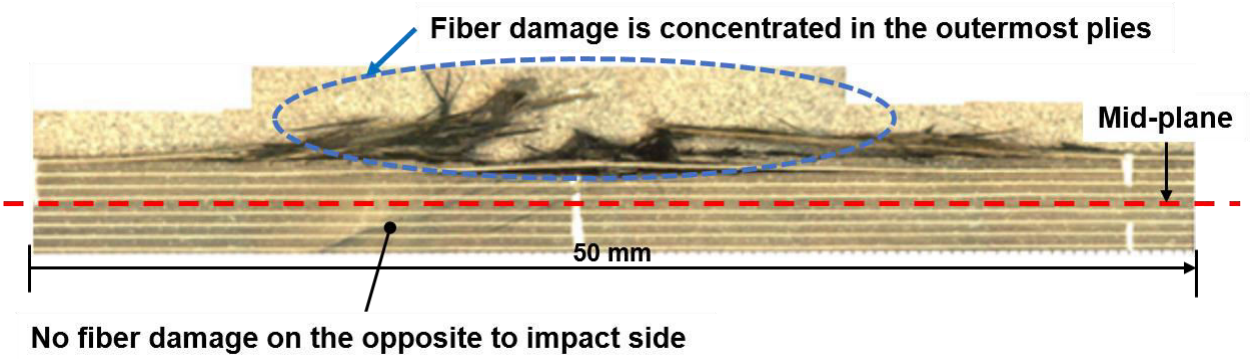

Figure 11. Sectional observation of a 32-ply quasi-isotropic ($[45/0/–45/90]_{4S}$) IM600/133 carbon/epoxy composite subjected to 40 kA peak lightning current [23].

5

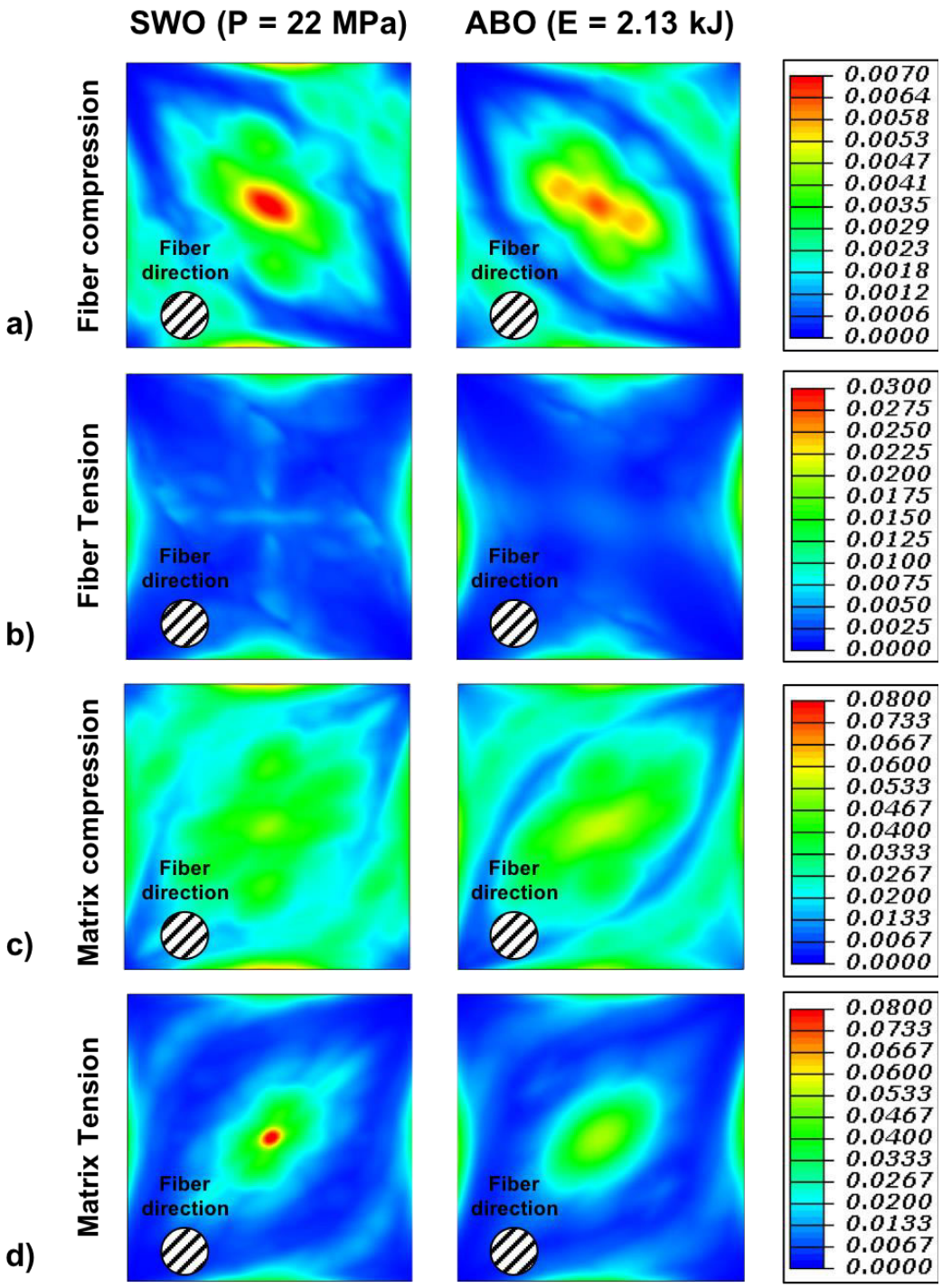

Figure 12. a) fiber compression, b) fiber tension, c) matrix compression, and d) matrix tension failure index distributions in the top AS4/3506 carbon/epoxy ply subjected to SWO and ABO, equivalent to a 124 kA peak current at $t = 5 \times 10^{-4}$s.

5

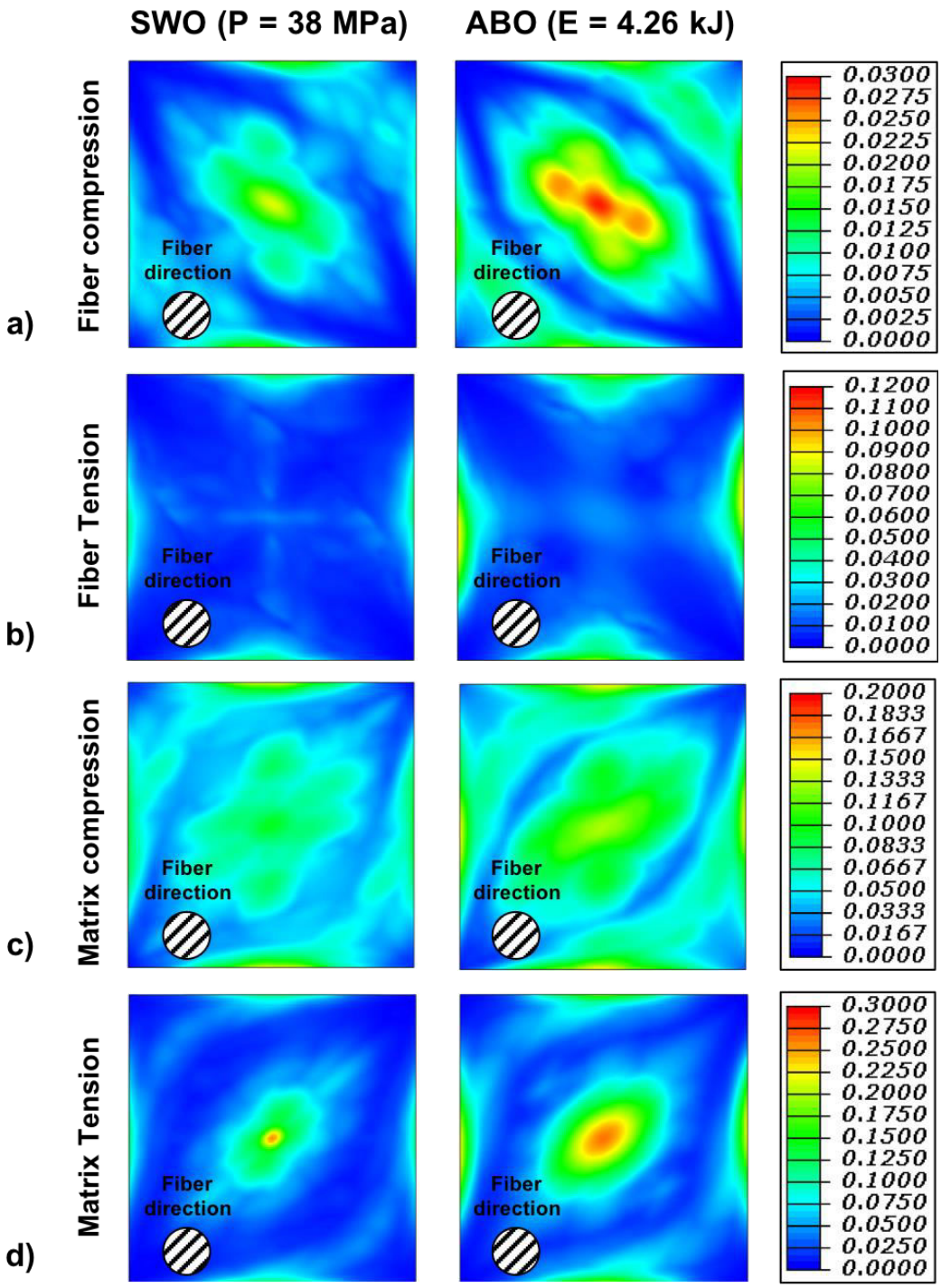

Figure 13. a) fiber compression, b) fiber tension, c) matrix compression, and d) matrix tension failure index distributions in the top AS4/3506 carbon/epoxy ply subjected to SWO and ABO, equivalent to a 247 kA peak current at $t = 5 \times 10^{-4}$s.

5

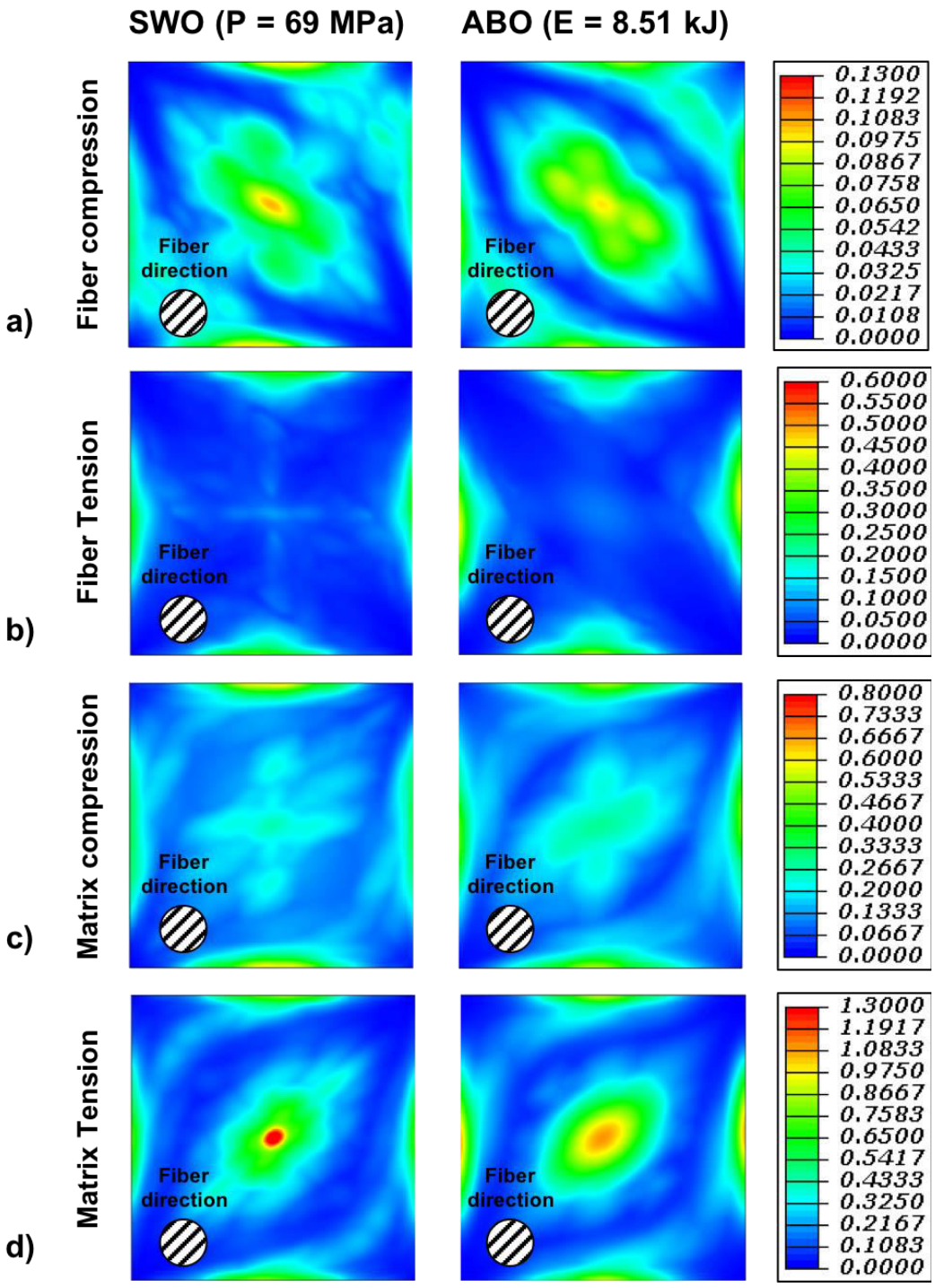

Figure 14. a) fiber compression, b) fiber tension, c) matrix compression, and d) matrix tension failure index distributions in the top AS4/3506 carbon/epoxy ply subjected to SWO and ABO, equivalent to a 494 kA peak current at $t = 5 \times 10^{-4}$s.

5

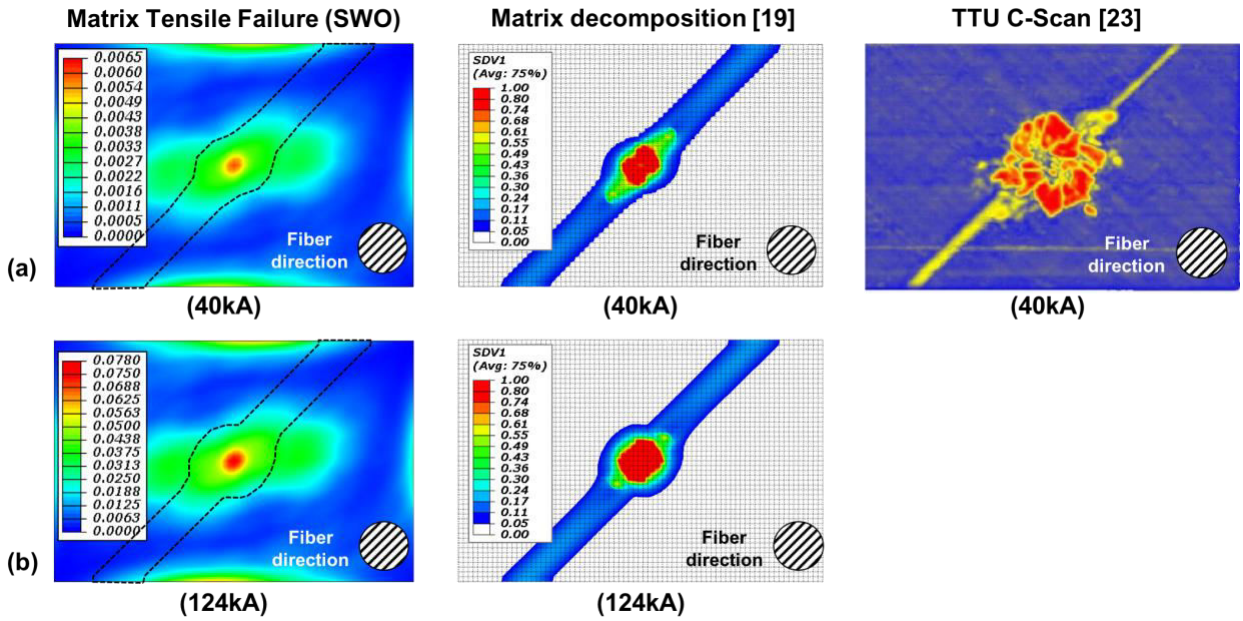

Figure 15. Comparison of matrix tension failure index distributions due to SWO, predicted matrix thermal decomposition [19], and through-transmission-ultrasonic (TTU) C-scan image [23] under a) 40 kA peak current and b) 150 kA peak current. The approximate matrix thermal decomposition domains (middle figures) are superimposed on the matrix tension failure index distributions (left figures).